

Impact of hardening law on the FEM prediction of residual stresses in Cu-Al wires

Alireza Dashti (✉ Alireza.dashti@insa-rouen.fr)

INSA Rouen: Institut National des Sciences Appliquées de Rouen <https://orcid.org/0000-0002-1726-565X>

Clément Keller

Benoit Vieille

Alain Guillet

Calogero Gallo

Anne-Marie Habraken



Laurent Duchêne

Research Article

Keywords: Wire drawing, Bimetallic composite, Copper, Aluminum, Finite element analysis, isotropic-kinematic hardening

Posted Date: November 30th, 2022

DOI: <https://doi.org/10.21203/rs.3.rs-2297442/v1>

License:   This work is licensed under a Creative Commons Attribution 4.0 International License.
[Read Full License](#)

Version of Record: A version of this preprint was published at The International Journal of Advanced Manufacturing Technology on April 4th, 2023. See the published version at <https://doi.org/10.1007/s00170-023-11315-2>.

Abstract

Near-surface axial tensile residual stresses (from manufacturing) are reportedly detrimental to the yield strength of cold-drawn wires. Therefore, a reliable evaluation of their magnitude is necessary. The size and geometry of electrical wires can pose challenges for experimental measurement of those residual stresses. For that reason, the finite element analysis can prove useful. However, great care must be taken with the right choice of strain hardening law for a sound assessment of residual stresses. Given the complex loading condition during cold drawing, cyclic loading arises through the wire cross section even in single-pass drawing. As a result, it is of crucial importance to account for associated backstresses. The current study makes a comparison between two different hardening laws' prediction of axial residual stress profiles in numerically cold-drawn Cu-Al composite wires of various Al volume fractions. The impact of die geometry on this prediction was also examined for a 25%Al-wire. To that end, a combined isotropic-kinematic law and a pure isotropic constitutive equation were considered. The results imply a possible overestimation of residual stresses by the pure isotropic model at relatively low Al volume fractions. The difference between the maximum magnitudes of tensile or compressive residual stresses (predicted by the two models) could be as large as about 100 MPa (larger than the yield strength of the starting materials). Furthermore, the tooling geometry minimally affects the prediction of the hardening models. In conclusion, backstresses are not to be overlooked for accurate estimations of drawing residual stresses at low Al volume fractions.

1. Introduction

Rising copper prices and its shortage [1] have led manufacturers to partially replace copper for different electrical applications. Lighter, cheaper and highly conductive aluminum is a good choice for partial replacement of pure copper. Cu-Al conductors of various compositions and configurations, such as busbar, rod and wire, are currently available. There are a variety of techniques for manufacturing these bimetallic composites. Rotary swaging, caliber rolling, hydrostatic extrusion, and wire drawing [2]–[5] are among them. Cold wire drawing is commonly used to manufacture copper-clad aluminum wires, abbreviated as CCA. Wire drawing involves reducing the cross-sectional area of a wire by pulling it through conical dies [6]. Non-uniform plastic deformation during this process gives rise to a triaxial residual stress state with radial, tangential and axial components [7].

Several researches have investigated the adverse effect of axial tensile residual stresses on the tensile strength and fatigue properties of cold-drawn wires. Atienza et al. [8] associate tensile surface residual stresses with the number of cycles to rupture of eutectoid steel wires. They suggest post-drawing treatments such as stabilizing, rolling and skin pass to enhance the wire's fatigue resistance against environmentally assisted cracking (EAC). Atienza and Elices [9] also argue that the aforementioned residual stress component lowers the yield strength of drawn steel wires. Dashti et al. [5] report that so-called architected Cu-Al composite wires have a higher yield strength than conventional CCA and full-copper counterparts in the as-drawn state (without heat-treatment). They ascribe it to lower-magnitude near-surface axial tensile residual stresses in architected wires. Ripoll et al. [10] attribute cracking of

drawn tungsten wires to surface residual stresses. They introduce an optimized die geometry and post-drawing bending operations to resolve the issue. It is common practice to use the finite element method (FEM) to predict wire drawing-induced residual stresses. Usually, isotropic hardening is adopted to describe the elastoplastic behavior of materials. However, it should be noted that isotropic hardening is generally not sufficient where non-proportional loading is involved [11]. Wire drawing is performed under complex loading conditions and cyclic loading happens even in single-pass drawing [12]. This can result in discrepancies between isotropic and kinematic hardening models' prediction of manufacturing residual stresses. Panteghini and Genna [12] suggest isotropic hardening as inadequate for accurate calculation of residual stress profiles in steel wires. They argue that an isotropic hardening law significantly overestimates residual stresses and, therefore, kinematic hardening must be adopted. Souza et al. [13] compare the numerically-predicted residual stress profiles of a cold-drawn AISI 1045 steel wire against those of neutron diffraction measurements. There is a considerable difference between the simulation and experimental results. They ascribe it to the fact that anisotropy and kinematic hardening are unaccounted for. Therefore, an appropriate choice of the hardening model seems inevitable for reliable evaluations of residual stresses.

The present work is an attempt to address the unavailability of literature on the hardening law-residual stress profile relationship in copper-clad aluminum wire or CCA. For that purpose, a numerical study was conducted to investigate how different hardening laws' predictions of residual stresses differ from one another as a function of the Cu/Al volume fraction and the tooling geometry (for the volume fraction 25%Al). The von Mises yield criterion was used with I- pure isotropic and II- combined isotropic-kinematic hardening models. The following sections provide further details about the materials, backstress calculation and the hardening model constants used to simulate wire drawing. Moreover, the residual stress profiles along the wire diameter are presented for all cases together with the corresponding contour plots. Finally, the results and implications are discussed and concluded.

2. Materials And Methods

2.1. Experimental procedure

Pure OFHC (Oxygen Free High Conductivity) copper and 99.5% pure Al were first annealed, for 3 hours at 500 and 300°C, respectively, to have a fully-recrystallized defect-free initial microstructure. In order to obtain the corresponding stress-strain curves, both materials were, then, tensile-tested using a 10 kN-universal testing machine 'MTS Criterion Model 43'. Tensile tests were carried out at room temperature, in a displacement-controlled mode. Specimens were strained at an initial strain rate of 0.004 s^{-1} to avoid possible viscous effects. A conventional 25 mm-gage length extensometer measured the axial strain. However, cold drawing often induces larger strains than the maximum total strain achievable in a tensile test (commonly between 20–30%), even during a single pass [14]. For instance, in this work, single-pass drawing of Cu-Al wires of different Al volume fractions, with an initial diameter of 12 mm, is numerically modelled for a cross-sectional area reduction of 20%. Starting Cu and Al phases were in the annealed

state with zero friction assumed at their interface. The preceding reduction ratio corresponds to a plastic strain of about 22% according to the following equation:

$$\eta = 2 \ln \frac{D_0}{D}$$

1

η , D_0 and D are, respectively, the amount of plastic strain, initial and final wire diameters. Therefore, both pure Cu and pure Al tensile curves were extrapolated to larger strains in order to provide a better description of the material behavior (Fig. 1). In order to estimate the backstress evolution with strain for copper, loading-unloading tensile tests were performed according to the procedure previously described in Ref [15], briefly explained as follows. Dumbbell-shaped samples with OFHC copper of a gage length of 18 and a total length of 70 mm were loaded and unloaded cyclically (Fig. 2) in a strain-controlled tensile test (strain rate = 0.0005 /s). Each loading-unloading loop was then analyzed in terms of its center and radius. The center is assumed to be related to the development of backstress in the material (kinematic hardening) whereas the radius is associated with the effective stress (representing isotropic hardening). A plastic strain offset of 0.0005 was considered to mark the end of elasticity during the unloading sequence. Backstress in pure copper arises due to heterogeneous dislocation structures (such as tangles, walls, cells) and strain incompatibilities between grains [15]. As reported in the literature, heavily strained pure copper develops a steady state microstructure [14]. Consequently, a mathematical formula predicting the saturation level was employed to extrapolate backstress [15]. An average of 50% was considered as the backstress portion of stress up to experimentally measured total strains of about 30%. Having assumed that a steady state reaches, the backstress evolution up to large strains was extrapolated for cold-drawing simulations. For aluminum, the backstress data was taken from the literature for an annealed commercially pure aluminum with the backstress portion of stress being about 16% [16]. The Bauschinger effect is more significant in low stacking fault energy materials. Pure Al has a higher stacking fault energy than pure Cu and, thus, a lower backstress portion of stress [17].

2.2. Numerical procedure

The finite element code, LAGAMINE, developed at the University of Liège, was used to model single-pass wiredrawing of an initially 12 mm-diameter Cu-Al wire whose cross-section decreases by 20% in one pass. As mentioned above, annealed Cu and Al phases with zero interfacial friction were assumed as the starting materials. Using the von Mises criterion, the simulations were run with both mixed isotropic-kinematic and pure isotropic hardening models for Cu-Al wires of three different volume fractions: 25%, 50%, and 75% Al. The commonly used Armstrong-Frederick equation (Equ. 2), after integration (Equ. 3), and the Voce (Equ. 4) equation (able to predict the stress saturation level) were fitted to the experimental data (Figs. 3 and 4) to identify the material parameters (listed in Table 2) for the kinematic and isotropic hardening models, respectively. Table 1 presents the parameters in the equations below.

$$\dot{X} = C_X (X_{sat} \dot{\epsilon}^{plastic} - \dot{\epsilon}^{plastic} X)$$

2

$$X = X_{sat}(1 - \exp(-C_X \cdot \dot{\epsilon}^{plastic})) \quad (3)$$

$$\sigma_F = \sigma_0 + K(1 - \exp(-n \cdot \dot{\epsilon}^{plastic}))$$

4

Table 1
The Armstrong-Frederick and Voce equation parameters.

Parameter	Description
\dot{X}	Backstress rate tensor
-	
C_X	Kinematic hardening saturation rate
X_{sat}	Kinematic hardening saturation value
$\dot{\epsilon}^{plastic}$	Plastic strain rate tensor
-	
$\dot{\epsilon}^{plastic}$	Equivalent plastic strain rate
X	Backstress tensor
-	
σ_F	Flow stress
σ_0	Yield stress
K	Hardening factor
n	Hardening exponent
$\epsilon^{plastic}$	Equivalent plastic strain

Figures 3 and 4 display the curve-fitting results for pure Cu and pure Al (over a strain range of 0-0.5) to obtain the isotropic and kinematic parameters (fitting constants) for the mixed isotropic-kinematic law. The fitting constants for both mixed and pure isotropic models are presented in Table 2.

Table 2
Armstrong-Frederick and Voce equation parameters (fitting constants).

Parameter	Mixed isotropic-kinematic		Pure isotropic	
	Cu	Al	Cu	Al
$C_X(MPa/s)$	8.3	77.5	-	-
$X_{sat}(MPa)$	180.7	22	-	-
$\sigma_0(MPa)$	22.7	78.9	45.3	93.9
$K(MPa)$	163.2	38.9	326.4	46.3
n	6.7	17.9	6.7	17.9

Given the symmetric configuration of the Cu-Al composite wires, a quarter of them with an initial length of 30 mm was created through the finite-element mesh generator, Gmsh [18], for all the volume fractions investigated here. The wires were entirely meshed via reduced-integration linear hexahedron elements with their outer surfaces covered with a layer of reduced-integration linear quadrilateral elements to model the wire-die contact. A wire drawing die of a semi-angle of 8° was also designed and meshed with triangular elements. The wire drawing assembly was then introduced to LAGAMINE through a Gmsh-LAGAMINE interface. Figure 5 shows the assembly including a quarter of a deformable 25%Al-CCA wire (assuming a perfect Cu-Al bond) together with a rigid body shell representing the interior of the die. The inner faces of the quarter were fixed one in the X- and the other in the Y-direction with the die restrained in all directions. A 50 mm-displacement was applied on the front end of the wire to move it through the die until the other end exits. The experimentally manufactured CCA wires in the authors' preceding studies [19], [20] were cold-drawn using a semi-industrial bench with powdered soap as the lubricant, whose friction coefficient is rather small, ranging between 0.033 and 0.061 [21]. Therefore, the friction coefficient was set to zero in the current simulations. Moreover, since the temperature rise during cold drawing was insignificant, the effect of viscosity and drawing velocity were assumed minimal. As already mentioned, the von Mises yield criterion was considered, without accounting for the potential intrinsic elastoplastic anisotropy of the materials (annealed pure Cu and Al). Backstress-induced anisotropy, alone, can provide accurate enough predictions of the residual stress profile in some cases [12].

Table 3 contains the elastic properties of Cu and Al.

Table 3
The Young's modulus (E),
shear modulus (G), and
Poisson's ratio (ν) values for
Cu and Al.

Parameter	Cu	Al
E (GPa)	128.8	66.2
G (GPa)	44	25
ν	0.31	0.33

The axial residual stress profile along the wire diameter was then plotted for the three volume fractions 25, 50, and 75% Al. A further investigation was carried out to determine how the tooling geometry (die angle and reduction ratio) could possibly affect the difference between the predictions of the axial residual stress profiles, with the above hardening models. The 25%Al-CCA wire was studied among the three volume fractions, for the reasons given later in the text. Accordingly, the 20% area reduction of the 25%Al-composite wire was achieved with 6° and 10° die semi-angles (in addition to the original 8°) in separate simulations. Additionally, the reduction ratio effect was examined within a range of 10–20%, with 5% steps (10, 15, and 20%), with a die angle of 8°. The axial residual stress profiles through the wire cross section were next plotted to show their dependence on the die design. The results and their implications will be discussed in the following paragraphs.

3. Results

Fig. 6 exhibits quarters of the above-mentioned CCA wires of different Al volume fractions, showing the evolution of axial stresses at a particular stage during drawing. The axial residual stress component developed in different cases (at the end of the drawing process) is profiled along the diameter of numerically drawn wires in Fig. 7 for comparison purposes. The paths, over which the profiles are plotted, were taken from the relatively uniform middle part of the contour, away from the ends to avoid possible edge effects. The Cu and Al phases are delineated in both Figs. 6 and 7.

As seen in Fig. 7, the smaller the Al volume fraction (core material) is, the more different (in terms of magnitude) the axial residual stress profiles predicted by pure isotropic and mixed isotropic-kinematic hardening models will be. The difference between the maximum tensile and compressive axial residual stresses of the two profiles may be as large as 100 MPa or even more for the 25%Al-CCA wire. However, the discrepancy diminishes as the Al core becomes larger in diameter (i.e. volume fractions, 50 and 75%).

Table 4 provides a comparison between the maximal values of tensile and compressive components of axial residual stress for different cases.

Table 4

Maximal values of axial residual stresses predicted by pure isotropic and mixed hardening models.

Axial residual stress (MPa)						
Maximum tensile residual stress				Maximum compressive residual stress		
CCA wire	<i>Isotropic-Kinematic</i>	<i>Pure isotropic</i>	Δ_T	<i>Isotropic-Kinematic</i>	<i>Pure isotropic</i>	Δ_C
25%Al-CCA	42.5	134.7	92.2	-89.8	-227.7	-137.9
50%Al-CCA	134.7	165.9	31.2	-140.2	-209.8	-69.6
75%Al-CCA	180.4	177.4	-3	-148.1	-187.9	-39.8

Figs. 9 and 10 illustrate the impact of die semi-angle (α in Fig. 8) and reduction ratio (R^2/R_0^2 as shown in Fig. 8) on the different hardening models' prediction of axial residual stresses (profiled along the diameter of the 25%-Al wire). The results were obtained according to the explanation given earlier in the subsection, 2.2. As mentioned in section 2, the effect of tooling geometry was investigated for the 25%Al-CCA wire. This choice was made in order to study the impact of die semi-angle and reduction ratio for the sample showing the greatest discrepancy between the pure isotropic and mixed hardening models' predictions (see table 4).

As seen in the above figures, the axial residual stress profiles overlap each other within both studied ranges of die semi-angle and reduction ratio. The difference between the maximum magnitude of tensile and compressive residual stresses, predicted by both hardening models, remain between 90–140 MPa for all cases. The residual stress distribution trend and slope, also, remains almost the same. As is shown in Figs. 9 and 10, a sharp variation of the axial residual stress arises in the copper phase of wires simulated with a pure isotropic hardening model. However, the distribution is relatively smooth in both phases for the wires with mixed isotropic-kinematic hardening. The difference between the two hardening models' prediction of axial residual stresses and the negligible impact of the tooling geometry on that will be discussed in the next section followed by the conclusions.

4. Discussion

As introduced earlier, even single-pass wire drawing involves cyclic loading and therefore backstress and kinematic hardening need to be accounted for. Thus, a proper estimation of residual stresses requires the

use of a realistic enough hardening model to correctly simulate the manufacturing process. Kinematic hardening is often found in conjunction with isotropic hardening [22]. As a result, a mixed isotropic-kinematic hardening model was adopted based on the experimental and literature data for copper and aluminum, respectively. The axial residual stress profiles from the wire drawing simulation of Cu-Al wires of different Al volume fractions (using mixed hardening) were then compared against those predicted by a pure isotropic hardening model as outlined above. In addition to that, the impact of die geometry (semi-angle and reduction ratio) on the different hardening models' prediction of axial residual stress was considered. The subsequent sections discuss the results.

4.1. Mixed vs pure isotropic hardening model: axial residual stress profiles

Axisymmetric forming operations, including wire drawing, cause residual stresses to develop since a material element tends to move faster through the die the farther it is from the tool-workpiece interface. Hence, residual stresses form due to elastic recovery after non-uniform plastic strains [23], [24]. When it comes to composite materials, differing mechanical properties of the components, such as yield strength (σ_0), also introduce some degree of deformation non-uniformity [25]. Figure 7 indicates that the 25%Al-CCA shows the most discrepant axial residual stress profiles (predicted by mixed and pure isotropic models) among the three volume fractions studied. This could be explained by two arguments. Firstly, the loading condition in cold drawing is cyclic as opposed to monotonic. The mixed hardening law employed here accounts for cyclic loading by reproducing the Bauschinger effect. Accordingly, the larger the volume fraction of aluminum, whose backstress portion of stress is significantly smaller than copper ($\approx 16\%$ vs $\approx 50\%$), the smaller the residual stress profile discrepancies will be. The mechanism through which kinematic hardening brings about lower-magnitude axial residual stresses with smoother variations can possibly be associated with the plastic-strain-induced anisotropy, represented by backstress. This anisotropy, arising from a translation of the yield surface, possibly lowers the heterogeneity of plastic deformation during wire drawing leading to reduced axial residual stresses with a regular distribution.

Secondly, the deformation heterogeneity during wire drawing extends through a greater thickness in the copper cladding of the 25%Al-CCA. Nevertheless, the plastic deformation non-uniformity evolves over a thinner copper sleeve with the increase of Al volume fraction (50 and 75%). Consequently, a less steep gradient arises in the copper phase from the wire surface to the Cu-Al interface. Therefore, the mixed and pure isotropic hardening models' prediction of magnitude and distribution of axial residual stresses, in the pure Cu sleeve, would not greatly differ from one another at smaller Cu volume fractions. This has interesting industrial implications for standard classes of copper-clad aluminum wires, containing 10–15% Al, [26] in the sense that a pure isotropic model can presumably predict residual stress with sufficient accuracy.

4.2. Die geometry and hardening law: 25%Al-CCA

As stated in “Materials and methods”, followed by the corresponding results in the previous section, 25%Al-CCA was chosen in order to look into how different hardening laws’ numerical prediction of axial residual stresses can potentially change as a function of the die geometry. The above specimen was opted because of showing a rather remarkable difference between the residual stress profiles depending on the hardening model used to simulate its drawing (isotropic-kinematic or pure isotropic). Wire drawing energy is composed of homogeneous, friction, and redundant work. Homogeneous work is the useful work to reduce cross section. Friction work was assumed insignificant as stated earlier. Redundant work occurs due to changes in the direction of flow of the metal in the die and causes internal shearing and distortion. The last component (redundant work) is closely related to the die geometry [6], [27].

According to Figs. 9 and 10, as explained in the “Results” section, varying the die semi-angle and reduction ratio, within common ranges, would negligibly change the axial residual stress profiles of 25%Al-CCA, predicted by both hardening models. The composite nature of the studied cold-drawn wires conceivably describes these numerical observations. This can be attributed to the fact that the mechanical incompatibility between the pure Cu and pure Al phases prevails any moderate changes of the tooling geometry in determining the axial residual stress profiles, irrespective of the hardening law. It may be argued that die geometry modifications, within above limits, slightly influences the redundant portion of the total energy of cold drawing of Cu-Al wires.

5. Conclusions

The present study is aimed at comparing pure isotropic and mixed isotropic-kinematic hardening models with respect to their estimation of axial residual stresses in numerically drawn Cu-Al composite wires of different Al volume fractions. Further to that, the impact of tooling geometry on the hardening laws’ prediction of axial residual stresses was investigated for a given volume fraction (25%Al). The conclusions are as follows:

- The higher the volume fraction of pure Cu is in copper-clad aluminum wires (the thicker the Cu sleeve), the more significantly mixed and pure isotropic hardening models will deviate from one another in terms of numerically predicted maximal values of axial residual stresses.
- A pure isotropic hardening model may provide sufficiently accurate estimates of axial residual stresses in CCA wires of relatively large Al volume fractions (70–90%) without needing to consider kinematic hardening
- The mechanical incompatibility between pure Cu and pure Al plays a more determining role than moderate die geometry modifications with regard to predicted axial residual stress profiles, regardless of the hardening model.

Declarations

Funding

The authors gratefully acknowledge the funding from The Region of Normandy.

Conflicts of interest

The authors declare that they have no conflict of interest.

Authors' contributions

Not applicable

Acknowledgements

The authors wish to thank the PhD students Carlos Rojas Ulloa and Ehssen Betaieb from the University of Liège's Department of Architecture, Geology, Environment and Constructions (ArGEnCo) for their kind help and technical advice with the finite element code "LAGAMINE".

References

1. B. W. Schipper, H.-C. Lin, M. A. Meloni, K. Wansleben, R. Heijungs, and E. van der Voet, "Estimating global copper demand until 2100 with regression and stock dynamics," *Resour. Conserv. Recycl.*, vol. 132, pp. 28–36, 2018.
2. L. Kunčická and R. Kocich, "Deformation behaviour of Cu-Al clad composites produced by rotary swaging," in *IOP Conference Series: Materials Science and Engineering*, 2018, vol. 369, no. 1, p. 012029.
3. J.G. Kim, M.I. Latypov, D.J. Lee, H.G. Jeong, J.B. Lee, S. Lee, H.S. Kim, "Plastic deformation behavior and microstructural evolution of Al-Core/Cu-Sheath composites in multi-pass caliber rolling," *Metall. Mater. Trans. A*, vol. 46, no. 1, pp. 260–269, 2015.
4. R. Srinivasan, "Study of the hydrostatic co-extrusion of aluminum and copper (computer simulation, residual stress).," 1984.
5. A. Dashti, C. Keller, B. Vieille, and A. Guillet, "Novel approach to optimize the mechanical properties of Cu-Al composite wires," *Int. J. Mater. Form.*, vol. 15, no. 3, pp. 1–10, 2022.
6. "Theory of wire drawing," 2007. <https://www.semanticscholar.org/paper/theory-of-wire-drawing/15716537d024c014844830fc8b1eccdb1bb7392c> (accessed Dec. 24, 2021).
7. J. M. Atienza, J. Ruiz-Hervias, and M. Elices, "The role of residual stresses in the performance and durability of prestressing steel wires," *Exp. Mech.*, vol. 52, no. 7, pp. 881–893, 2012.
8. J. M. Atienza, M. Elices, J. Ruiz-Hervias, L. Caballero, and A. Valiente, "Residual stresses and durability in cold drawn eutectoid steel wires," *Met. Mater. Int.*, vol. 13, no. 2, pp. 139–143, 2007.
9. J. M. Atienza and M. Elices, "Influence of residual stresses in the tensile test of cold drawn wires," *Mater. Struct.*, vol. 36, no. 8, pp. 548–552, 2003.
10. M. R. Ripoll, S. M. Weygand, and H. Riedel, "Reduction of tensile residual stresses during the drawing process of tungsten wires," *Mater. Sci. Eng. A*, vol. 527, no. 13–14, pp. 3064–3072, 2010.

11. N. S. Ottosen, "Nonlinear kinematic hardening under non-proportional loading," Risoe National Lab., 1979.
12. A. Panteghini and F. Genna, "Effects of the strain-hardening law in the numerical simulation of wire drawing processes," *Comput. Mater. Sci.*, vol. 49, no. 2, pp. 236–242, 2010.
13. T. F. de Souza, C. A. T. Soares, J. Zottis, R. M. Nunes, A. da S. Rocha, and T. Hirsch, "Comparison between Neutron Diffraction measurements and numerical simulation of residual stresses of a Wire-Drawing process," *Mater. Res.*, vol. 16, pp. 508–514, 2013.
14. N. Q. Chinh, G. Horváth, Z. Horita, and T. G. Langdon, "A new constitutive relationship for the homogeneous deformation of metals over a wide range of strain," *Acta Mater.*, vol. 52, no. 12, pp. 3555–3563, 2004.
15. G. Marnier, C. Keller, and L. Taleb, "Fatigue of OFHC pure copper and 316L stainless steel subjected to prior tensile and cyclic prestrains," *Int. J. Fatigue*, vol. 91, pp. 204–219, 2016.
16. S. Gao, K. Yoshino, D. Terada, Y. Kaneko, and N. Tsuji, "Significant Bauschinger effect and backstress strengthening in an ultrafine grained pure aluminum fabricated by severe plastic deformation process," *Scr. Mater.*, vol. 211, p. 114503, 2022.
17. A. A. Saleh, E. V. Pereloma, B. Clausen, D. W. Brown, C. N. Tomé, and A. A. Gazder, "On the evolution and modelling of lattice strains during the cyclic loading of TWIP steel," *Acta Mater.*, vol. 61, no. 14, pp. 5247–5262, Aug. 2013, doi: 10.1016/j.actamat.2013.05.017.
18. "Gmsh: a three-dimensional finite element mesh generator with built-in pre- and post-processing facilities." <https://gmsh.info/> (accessed Nov. 07, 2022).
19. C. Keller, F. Moisy, N. Nguyen, S. Eve, A. Dashti, B. Vieille, A. Guillet, X. Sauvage, E. Hug, "Microstructure and mechanical properties characterization of architected copper aluminum composites manufactured by cold-drawing," *Mater. Charact.*, vol. 172, p. 110824, 2021.
20. A. Dashti, C. Keller, B. Vieille, A. Guillet, and C. Bouvet, "Experimental and Finite Element Analysis of the Tensile Behavior of Architected Cu-Al Composite Wires," *Materials*, vol. 14, no. 21, p. 6305, 2021.
21. "Friction in: WIRE DRAWING," *Ind. Lubr. Tribol.*, vol. 3, no. 3, pp. 26–26, Jan. 1951, doi: 10.1108/eb052102.
22. E. Rouhaud, A. Ouakka, C. Ould, J. L. Chaboche, and M. François, "Finite elements model of shot peening, effects of constitutive laws of the material," in *Proceedings ICSP-9, Paris, France*, vol. 1, 2005.
23. M. M. Dehghani, "Mechanical Engineering Department," *ESDA 1996 Compos. Mater. Manuf. Fatigue*, vol. 3, p. 159, 1996.
24. M. M. A. Dehghani, Computer simulation of hydrostatic co-extrusion of bimetallic compounds. Louisiana State University and Agricultural & Mechanical College, 1987.
25. T. Marr, J. Freudenberger, D. Seifert, H. Klauß, J. Romberg, I. Okulov, J. Scharnweber, A. Eschke, C.G. Oertel, W. Skrotzki, U. Kühn, "Ti-Al composite wires with high specific strength," *Metals*, vol. 1, no. 1, pp. 79–97, 2011.

26. "Standard Specification for Copper-Clad Aluminum Wire." <https://www.astm.org/b0566-04ar21.html> (accessed Sep. 20, 2022).
27. R. Srinivasan and C. S. Hartley, "Coextrusion," 2005.

Figures

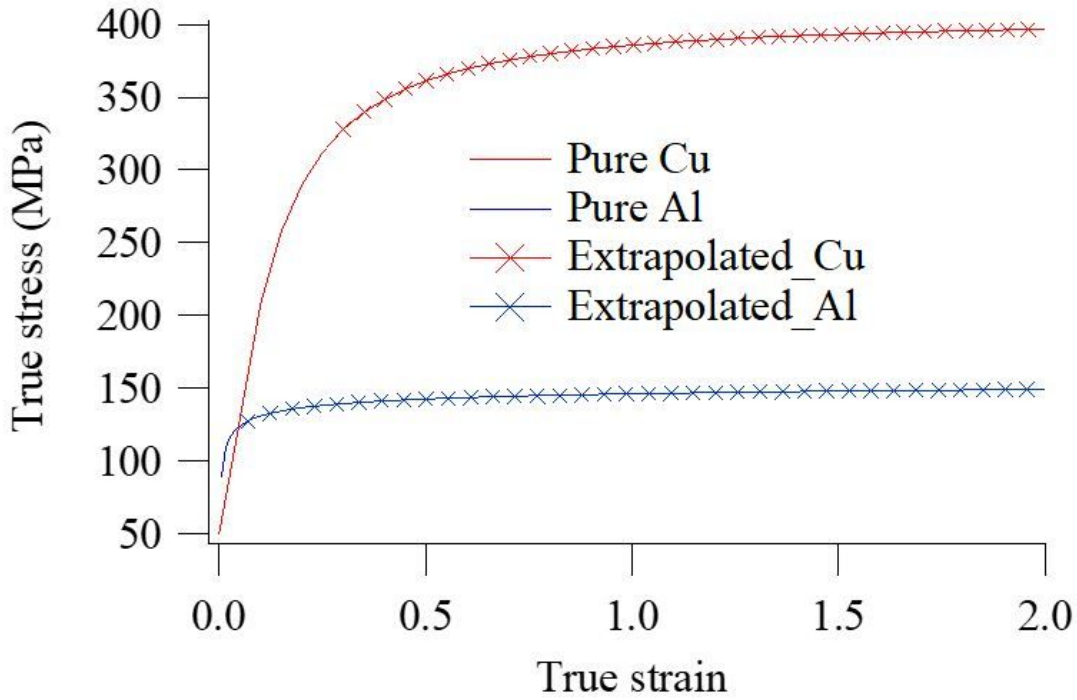
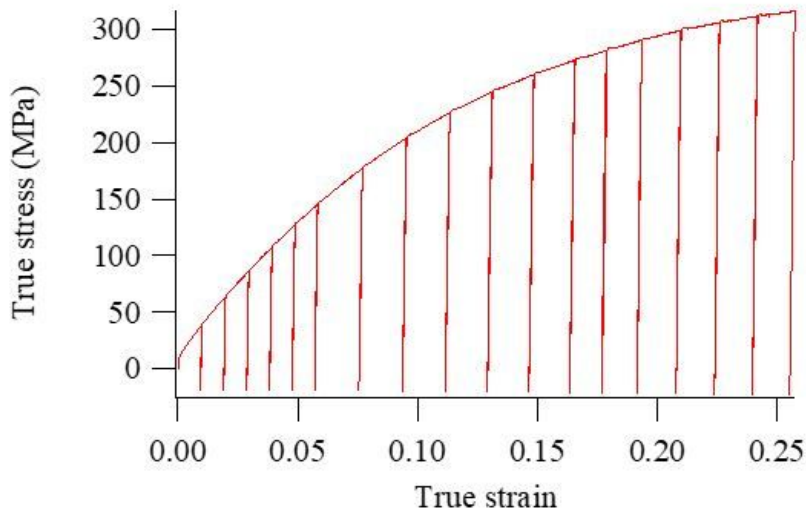
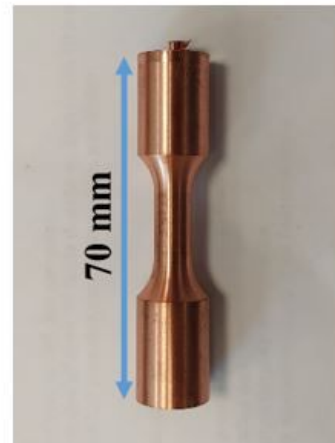


Figure 1

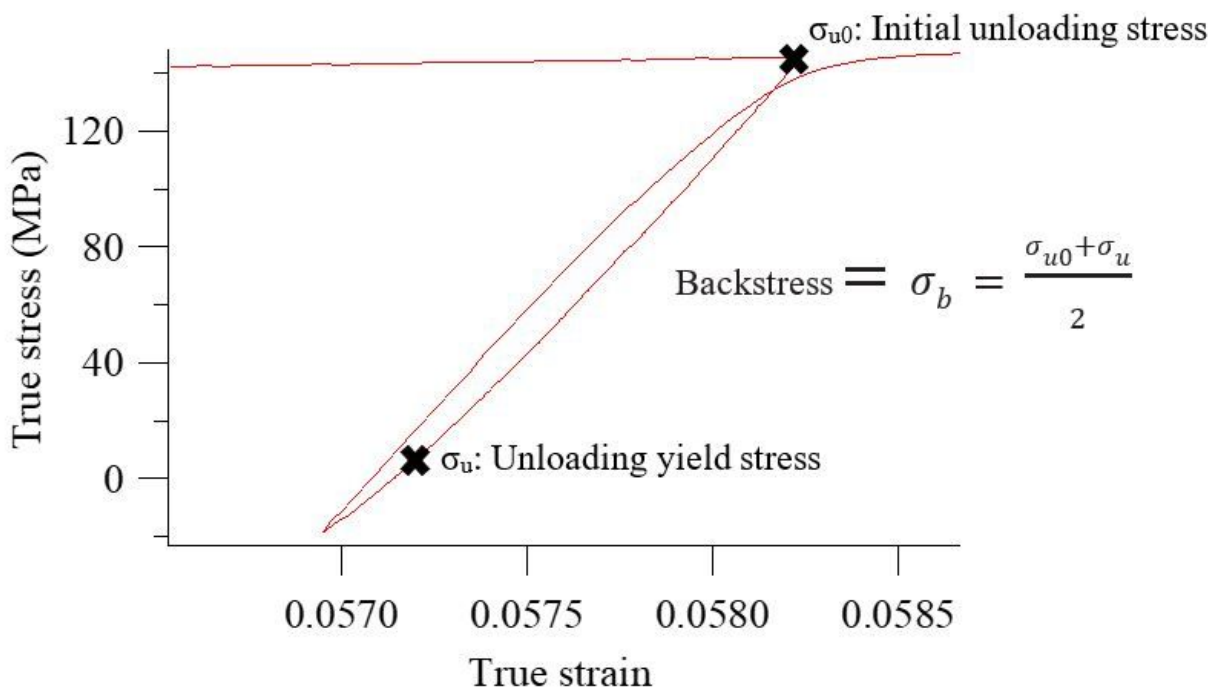
Experimental pure Cu and pure Al stress-strain curves



(a)



(b)



(c)

Figure 2

(a) Pure Cu loading-unloading curve, (b) test specimen and (c) backstress calculation

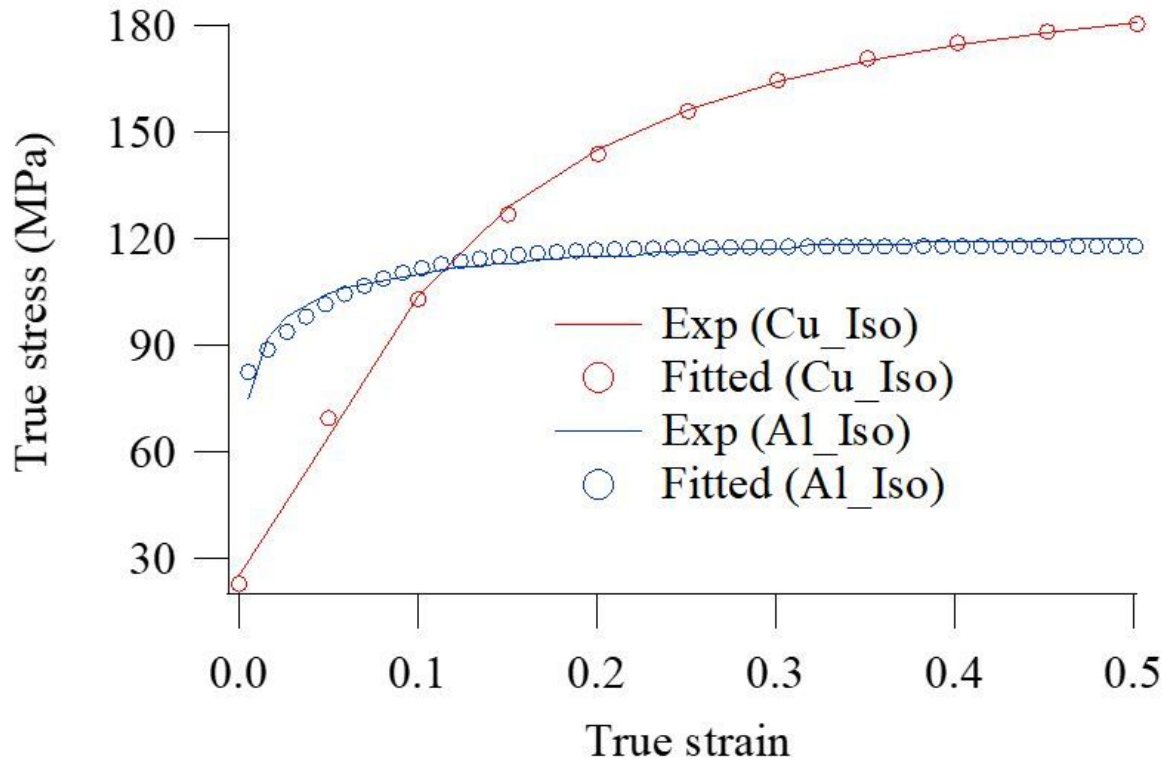


Figure 3

Experimental and fitted curves of the isotropic segment of pure Cu and pure Al stress-strain curves

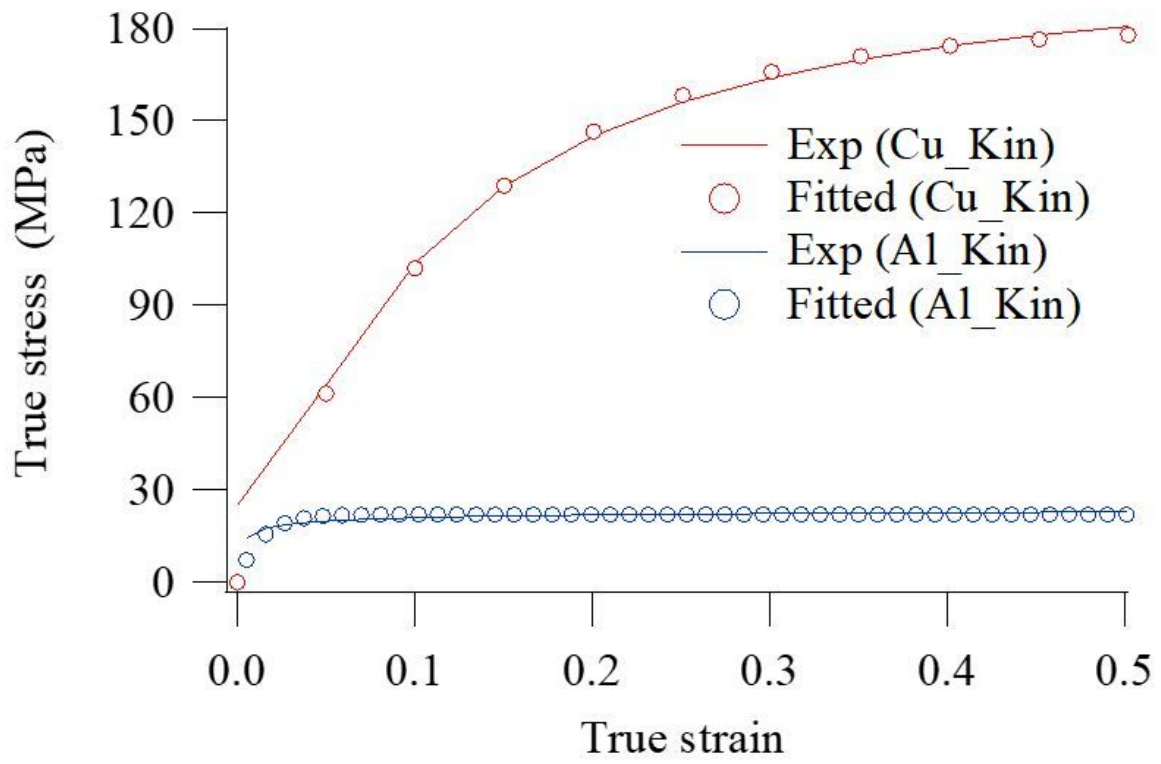


Figure 4

Experimental and fitted curves of the kinematic segment of pure Cu and pure Al stress-strain curves

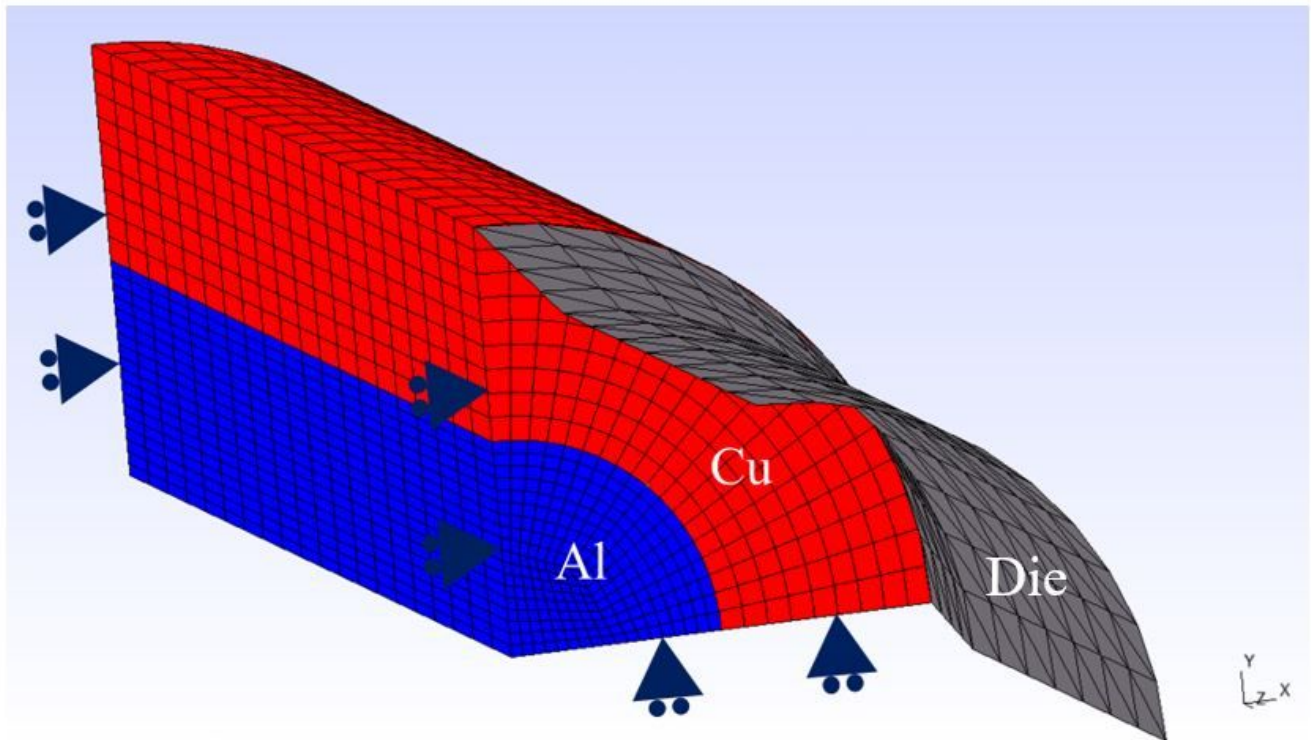


Figure 5

Wire drawing assembly of a 25%-Al CCA along with the die interior

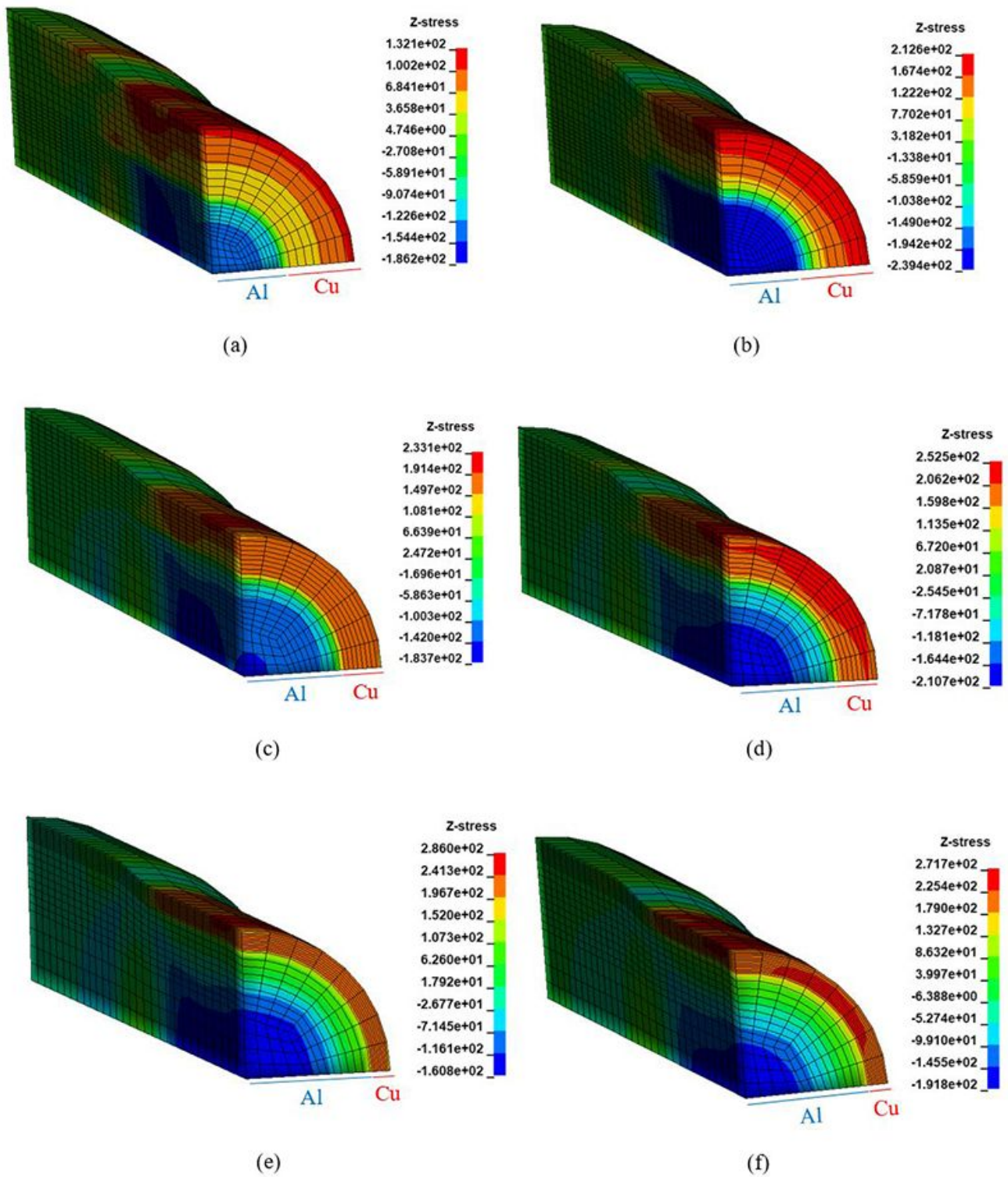


Figure 6

Cold-drawing of Cu-Al composite wires (CCA) of different volume fractions (stresses in MPa):

(a) 25% Al-CCA (isotropic-kinematic hardening) and (b) 25% Al-CCA (pure isotropic hardening)

(c) 50% Al-CCA (isotropic-kinematic hardening) and (d) 50% Al-CCA (pure isotropic hardening)

(e) 75% Al-CCA (isotropic-kinematic hardening) and (f) 75% Al-CCA (pure isotropic hardening)

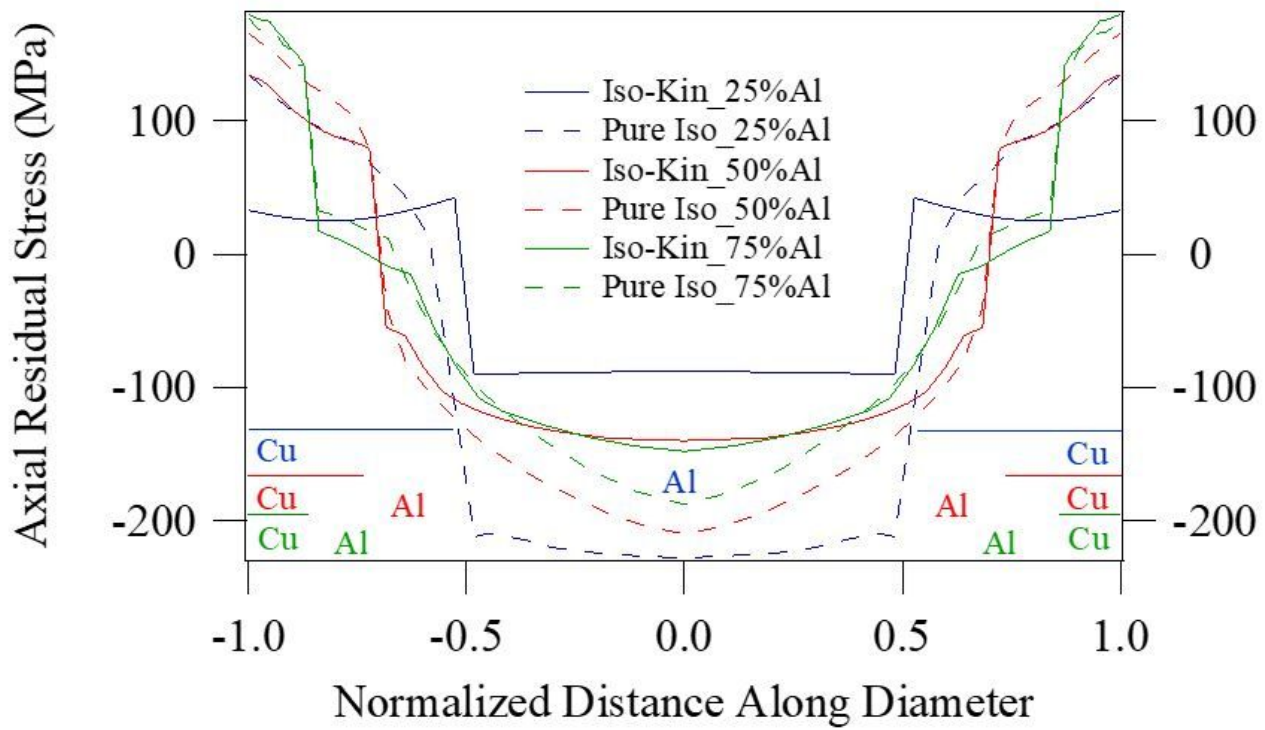


Figure 7

Axial residual stress profiles of numerically cold-drawn Cu-Al composite wires (CCA) of different volume fractions with different hardening models

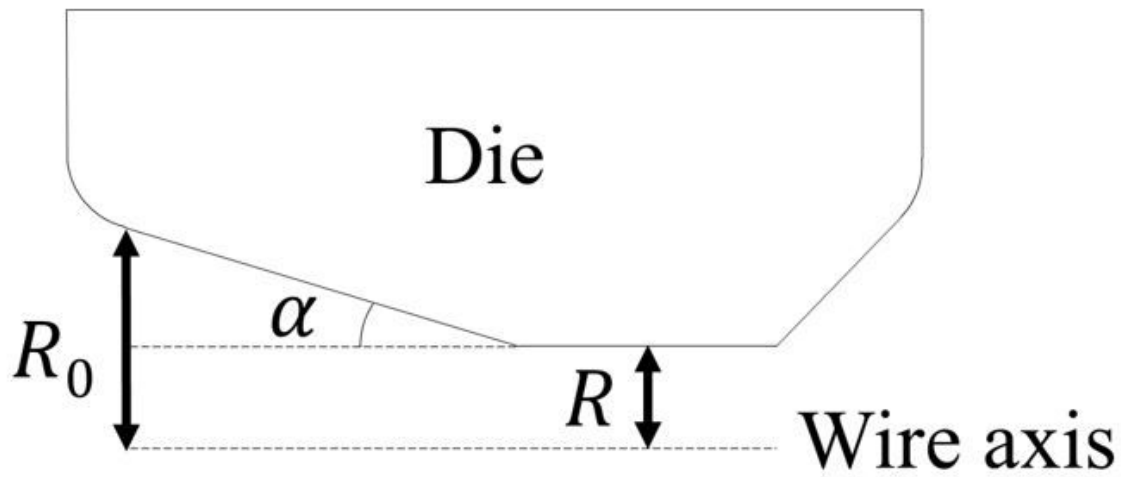


Figure 8

Simple schematic of the die semi-angle, initial and final radii of the wire

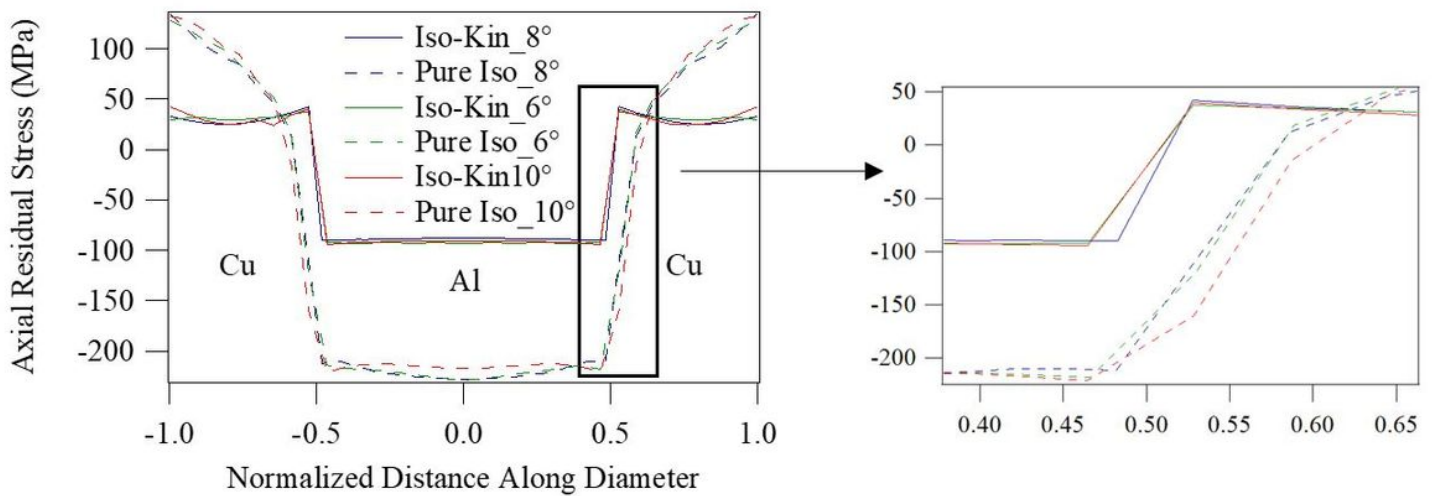


Figure 9

Axial residual stress profiles of 25%Al-composite wires (CCA), numerically cold-drawn with different die angles and different hardening models (reduction ratio = 20%)

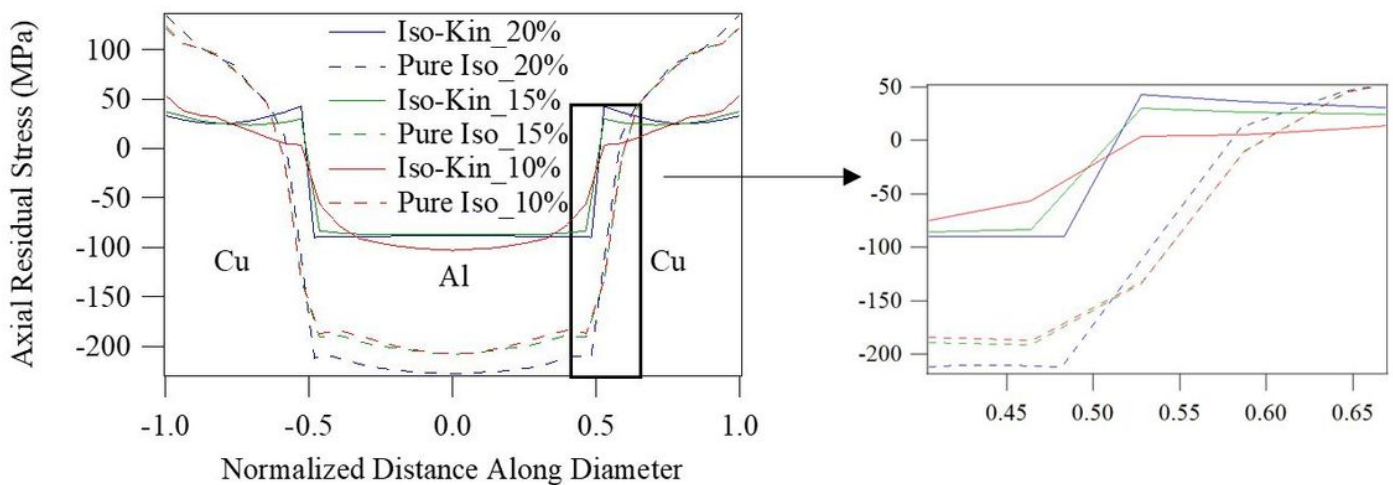


Figure 10

Axial residual stress profiles of 25%Al-composite wires (CCA), numerically cold-drawn with different reduction ratios and different hardening models (die semi-angle = 8°)